

## **A MODIFIED DOUBLE LAP-SHEAR TEST AS A MEAN TO MEASURE INTRINSIC PROPERTIES OF ADHESIVE JOINTS**

**D.-A. Mendels, S. A. Page, Y. Leterrier, J.-A. E. Manson<sup>†</sup>**

Laboratoire de Technologie des Composites et Polymères (LTC)  
Ecole Polytechnique Fédérale de Lausanne (EPFL)  
CH-1015 Lausanne, Switzerland

**J. A. Nairn**

Material Science and Engineering  
University of Utah  
Salt Lake City, Utah 84112, USA

**Keywords:** modified double-lap shear, internal stresses, modified shear-lag, shape functions

### **ABSTRACT**

A new double lap-shear sample geometry suppressing the use of arms and working in compression is introduced. This geometry is not only intended to control the thickness of the adhesive layers and obtain sharp edges, but also to limit to a considerable extent the occurrence of a peel stress. This test is analyzed through a modified shear-lag theory including internal stresses resulting from the cure shrinkage of thermosetting resins and different coefficient of thermal expansion of the adhesive and adherents. This theory is validated using finite element analysis, and expanded to describe the case of imperfect joint failure. Such a phenomenon is present in most adhesive joints where the strength of the adhesive is reached before the interface fails, due to the presence of internal stresses.

### **INTRODUCTION**

Advanced composite materials are widely used in applications such as aircraft and automotive industry due to their high strength-to-stiffness ratio and high corrosion resistance. Their use as structural materials often requires that the polymer based composite be attached to another structure, by means of bolted joints, or more generally an adhesive layer, because of unavoidable stress concentrations. Therefore, an adhesive bonded structure generally consists of three components of different mechanical properties, namely the two adherents and the adhesive layer. Much concern has been paid in describing the mechanical response of such assembled system, including their behavior under bending, tension and shear. The problem of shear failure of interfaces addresses several applications such as metal to polymer composite bonding, metal to metal brazing or composite interlaminar failure. This problem is generally solved by four distinct routes, namely:

- i. the shear strength criterion
- ii. the local shear strain criterion
- iii. the stress intensity factor

---

<sup>†</sup> to whom correspondence should be addressed

iv. or the (strain) energy release rate.

These methods all have in common that they require a determination of the stress tensor of the system. However, because of the material non-homogeneity and the geometric complexity of the medium, the exact analytical treatment of the related structural problem is hopelessly complicated. The existing analytical solutions have, therefore, been carried out under certain simplifying assumptions in formulating the problem.

The strength of an adhesive joint is not a property of the adhesive alone but is a system property depending on adherents, the adhesive, the joint geometry, preparation and service (or test) conditions [1]. The most widely used test methods can be classified as general lap-shear tests. Early attempts, including those by Volkersen [2] or Goland and Reissner [3], to describe the stress field in the simple lap-shear geometry, consisting of two plates bonded by a glue film, have revealed the existence of a peel stress generated by flexure of the adherents due to misalignment of the parts. Its magnitude and geometric variations between samples were found to strongly reduce the reliability of the test results. It is indeed particularly difficult to manufacture samples with a controlled bond thickness. Furthermore, the effects of a glue meniscus and the initial stress state in the adhesive layer were generally ignored. Internal stresses resulting from cure shrinkage of thermosetting polymers and different coefficients of thermal expansion between the adhesive and the adherents during cool-down have indeed proven to play an important role in the adhesive performance of model systems [4]. However, in order to illustrate these effects, an alternative lap-shear test geometry, which minimizes sample preparation difficulties and the development of complex stress states, is required.

This study introduces a new lap-shear test geometry. The proposed modified double-lap shear specimen (MDLS) enables a tight control of the thickness of the adhesive layers with sharp edges, and introduces the possibility to mold several samples at once. The stress state in the MDLS, including internal stresses, is obtained from a modified shear lag-theory. It is further compared to Finite Element Analysis (FEA) results, and shape functions are found. The model is finally expanded to account for joint imperfections, such as microcracking, and compared to experimental values obtained in related work.

## TEST GEOMETRY

By contrast with traditional lap-shear design, the new geometry consists of the central part of a double lap-shear specimen and the inner adherent is pushed in, therefore limiting, to a considerable extent, the occurrence of peel stresses. **Fig 1** presents the geometry for solving for stresses in a double lap-shear specimen. The system is shown with 3 constituents: an inner plate of thickness  $2t_1$ , with Young modulus  $E_1$  and Poisson's ratio  $\nu_1$ ; two adhesive layers of thickness  $t_2$  and elastic properties  $E_2$ ,  $\nu_2$ ; and two outer plates of thickness  $t_3$  and elastic properties  $E_3$ ,  $\nu_3$ . The boundary conditions are defined by a simple compression on the inner plate of magnitude  $\sigma_0$  while the two outer plates are simply supported. The origin of axis system (x,y,z) is on the midplane of the plate midway between the top and bottom surfaces. The problem is symmetrical about the y-axis, thus only half of the system needs to be analyzed (which indeed shows the advantage of automatically having a zero shear stress at  $x=0$ ).

In the following, the inner plate is labelled 1, the adhesive layer 2, and the outer plate 3. The shear-lag analysis consists in determining the three averaged axial stresses  $\langle \sigma_{yy}^{(1)} \rangle$ ,  $\langle \sigma_{yy}^{(2)} \rangle$  and  $\langle \sigma_{yy}^{(3)} \rangle$  in the layers, and the interfacial shear stresses  $\tau_1$  (layer 1/layer 2),  $\tau_2$  (layer 2/layer 3).

## THEORY

A modified shear-lag theory was recently introduced by Nairn for determining stresses in multi-layered composite structure of  $n$  orthotropic layers of thickness  $t_i = x_i - x_{i-1}$  [5]. Based on analysis of the most common assumptions used in shear-lag models, it was proposed that an optimal shear-lag analysis can be derived by assuming the shear stresses are product of two function, one which depends only on  $x$  and one which depends only on  $y$ . A modified shear-lag method was developed by introducing shape function, like in the case of the cylindrical and platelet geometry [6]. The shape function represents assumptions about the  $x$  dependence of the stresses; the shear-lag analysis solves for the  $y$  dependence.

Eventually a system of  $(n-1)$  equations with  $(n-1)$  unknowns  $\tau_{xy}(x_i)$  is obtained, which can be solved by writing the shear stresses between consecutive layers as a vector and determining the roots of the system matrix (i.e. Eigenvalues + Eigenvectors). The following presents the solution to the case of  $n=3$  layers for the double lap-shear specimen.

The problem is solved through the system of equations:

$$\mathbf{A} \frac{\partial^2 \boldsymbol{\tau}}{\partial z^2} - \mathbf{B} \boldsymbol{\tau} = 0 \text{ where } \boldsymbol{\tau} = \begin{pmatrix} \tau_1 \\ \tau_2 \end{pmatrix} \quad [1]$$

where  $\mathbf{A}$  and  $\mathbf{B}$  are given by:

$$\mathbf{A} = \begin{pmatrix} \frac{t_1 \langle z_1 R_1 \rangle}{G_{xy}^{(1)}} + \frac{t_2}{3G_{xy}^{(2)}} & \frac{t_2}{6G_{xy}^{(2)}} \\ \frac{t_2}{6G_{xy}^{(2)}} & \frac{t_2}{3G_{xy}^{(2)}} + \frac{t_3 \langle z_3 L_3 \rangle}{G_{xy}^{(3)}} \end{pmatrix}; \quad \mathbf{B} = \begin{pmatrix} \frac{1}{E_y^{(1)} t_1} + \frac{1}{E_y^{(2)} t_2} & -\frac{1}{E_y^{(2)} t_2} \\ -\frac{1}{E_y^{(2)} t_2} & \frac{1}{E_y^{(2)} t_2} + \frac{1}{E_y^{(3)} t_3} \end{pmatrix} \quad [2]$$

$z_i$  being the local  $x$  coordinate,  $R_i$  and  $L_i$  the right and left shape function of layer  $i$  respectively.

For matrix  $\mathbf{A}$ , the shape functions in the thin adhesive layer have been assumed to be linear but, for now, the right shape function in layer 1 and the left shape function in layer 3 have been left undetermined. The solution of Equation [1] is:

$$\tau_i = -\sum_{j=1}^2 [C_{j+} \exp(\lambda_j y) + C_{j-} \exp(-\lambda_j y)] p_{ji} \quad [3]$$

where  $p_{ji}$  is the  $i$ th component of the eigenvector  $\bar{p}_j$  associated to the eigenvalue  $\lambda_j^2$  of the matrix  $\mathbf{M}$ :

$$\mathbf{M} = \mathbf{A}^{-1} \mathbf{B} \quad [4]$$

Axial stresses in the 3 layers are obtained from stress equilibrium:

$$\frac{\partial \langle \sigma_y^{(1)} \rangle}{\partial y} = -\frac{\tau_1}{t_1}; \quad \frac{\partial \langle \sigma_y^{(3)} \rangle}{\partial y} = \frac{\tau_2}{t_3} \quad [5]$$

and the following boundary conditions:

$$\begin{aligned} \sigma_y^{(1)} \Big|_{y=L/2} &= -\sigma_0 \\ \sigma_y^{(1)} \Big|_{y=-L/2} &= 0 \\ \sigma_y^{(2)} \Big|_{y=\pm L/2} &= 0 \end{aligned} \quad [6]$$

This gives, upon integration on  $y$ :

$$\begin{aligned} \sigma_y^{(1)} &= C_1 + (C_{1+} e^{\lambda_1 y} - C_{1-} e^{-\lambda_1 y}) \frac{P_{11}}{\lambda_1 t_1} + (C_{2+} e^{\lambda_2 y} - C_{2-} e^{-\lambda_2 y}) \frac{P_{21}}{\lambda_2 t_1} \\ \sigma_y^{(2)} &= C_2 + (C_{1+} e^{\lambda_1 y} - C_{1-} e^{-\lambda_1 y}) \frac{P_{12} - P_{11}}{\lambda_1 t_2} + (C_{2+} e^{\lambda_2 y} - C_{2-} e^{-\lambda_2 y}) \frac{P_{22} - P_{21}}{\lambda_2 t_2} \\ \sigma_y^{(3)} &= C_3 - (C_{1+} e^{\lambda_1 y} - C_{1-} e^{-\lambda_1 y}) \frac{P_{12}}{\lambda_1 t_3} - (C_{2+} e^{\lambda_2 y} - C_{2-} e^{-\lambda_2 y}) \frac{P_{22}}{\lambda_2 t_3} \end{aligned} \quad [7]$$

The integration constants of  $\langle \sigma_y^{(i)} \rangle$  are labelled  $C_i$  and determined using the far field stress hypothesis. If  $l$  tends towards infinite, the stresses tend to become symmetric vs. the centre of the assembly  $y=0$ , i.e. the solution tends towards that for symmetrical loading case. One then finds:

$$C_i = E_i \left( \frac{\sigma^*}{E^*} + (\alpha^* - \alpha_i) \Delta T \right) \quad [8]$$

where

$$\begin{aligned} E^* &= \frac{E_1 t_1 + E_2 t_2 + E_3 t_3}{t_1 + t_2 + t_3} \\ \sigma^* &= -\frac{t_1 \sigma_0}{t_1 + t_2 + t_3} \\ \alpha^* &= \frac{\alpha_1 E_1 t_1 + \alpha_2 E_2 t_2 + \alpha_3 E_3 t_3}{E^* (t_1 + t_2 + t_3)} \end{aligned} \quad [9]$$

It is important to notice that all the information on internal stresses is introduced via the constants  $C_i$ .

### Shape Functions

Two constants appear in matrix  $\mathbf{A}$  ( $\langle z_1 R_1 \rangle$  and  $\langle z_3 L_3 \rangle$ ). These two constants are the average values of shape functions describing the  $x$ -dependence of shear stress in the inner and outer plates respectively. Interestingly, the best fitting values were found close to:

$$\langle z_1 R_1 \rangle = \frac{E_1 t_1}{E_1 t_1 + E_2 t_2 + E_3 t_3}; \quad \langle z_3 L_3 \rangle = \frac{E_3 t_3}{E_1 t_1 + E_2 t_2 + E_3 t_3} \quad [10]$$

The shape functions chosen in the present are simple hyperbolic functions of  $1/z_i$ . In the present work, the adhesive shape functions were simply assumed to be linear; this assumption is reasonable because of the low adhesive film thickness. The shear-lag analysis is shown to compare well with FEA in **Fig 2**. The use of shape functions increases the accuracy of the analysis in **Fig 2**, and it can be seen that all energetic approaches would be very close. Nevertheless, due to the shear-lag assumptions, the shear stress does not vanish at the end of the joint, which involves an error when considering the maximum shear stress. However, this error becomes small when the Young's moduli ratio is increased.

### Effects of Internal Stresses

**Fig 3-4** illustrate two significant effects of internal stresses. While their influence is negligible on the adherents, it is marked in the adhesive layer. In terms of axial stress, a tensile residual stress builds up during cool down; its contribution to Von Mises shear stress is sufficient to induce microcracking of the adhesive. In terms of shear, the amount of interfacial shear generated by internal stress can be large. It is shown that, given an external load, the interfacial shear is increased with the level of internal stresses. The solution of the problem is easily recast as function of  $C_i$  which include the internal stresses contribution, so that it is possible to separate the contributions of applied load and internal stresses to the true local shear strength  $\tau_0$ . Eventually, with  $\tau_{exp}$  the shear stress due to applied load, one obtains

$$\tau_0 \propto \tau_{exp} + \chi \Delta T \quad [11]$$

where  $\chi$  is a positive parameter defined by elastic and geometric properties of the system.

The reader is referred to the experimental part of this work in ref. [7], in which the amount of internal stress was changed by process tailoring without affecting the surface thermodynamics nor the mechanical properties of the adhesive layer. It clearly evidenced that the true local bond strength was not affected by the process, i.e.  $\tau_0$  calculated within the formalism

presented here was constant, whereas the experimental failure loads were drastically moved towards lower values when the level of internal stresses increased.

## RESULTS AND DISCUSSION

A typical force vs. displacement curve, representative of the tests achieved with constituents of properties given by **Table I**, is presented in **Fig 5**. The temperature difference for this epoxy was such that  $\Delta T = -142^\circ\text{C}$ , and the applied load of  $\sigma_0 = 50\text{MPa}$  is representative of experimental results.

A deviation from elastic linearity is observed at point A during loading of the sample before first failure occurs (at C). The force vs. displacement curve then increases again (D to E) in a non-linear manner before the final failure of the sample is achieved.

Internal cohesive microcracking of the epoxy adhesive was clearly observed in fracture surfaces by means of scanning electron microscopy. The same phenomenon had already been reported for epoxy adhesive joints in standard double-lap shear geometries [8]. These microcracks are initiated by the high stress state induced in the adhesive layer by both axial and shear stresses and have an orientation of ca.  $45^\circ$ .

Let us consider a damaged zone of length  $d$  as shown in **Fig 6**. As a first approximation, it is possible to consider that the shear modulus of the adhesive, and thereby its Young modulus too, are reduced by transverse cracking. This hypothesis is well supported by the stress-strain curves one obtains in such a case, showing a decrease of the effective modulus of the joint. Under this hypothesis, the stresses of the system are obtained straightforwardly by assuming two zones with distinct mechanical properties of the adhesive, and requiring stresses to be continuous over these two zones. The basic stresses are obtained as in the case of the undamaged MDLS, treating the two zones separately and let stresses be continuous over zones.

In the frame of the MDLS system used up to this point, **Fig 7** shows the distribution of stresses if the Young's modulus is assumed to be decreased by 90% in the damaged zone.

Microcracks severely reduce the mechanical properties of the joints and, as a consequence, the maximum shear stress concentration is following the microcracking progression, rather than staying at the bond extremity. Microcracking progresses along the joint until the Von Mises shear stress in the center of the adhesive is low enough. As the undamaged length of joint is reduced, the maximum interfacial shear stress is decreased. At the maximum force, the maximum shear stress is located near the end of the microcracking length and reaches the interfacial shear strength of the joint. Fracture is thus initiated at this location and, from this point onwards, propagates along the interface.

As it was outlined previously, microcracking phenomenon is strongly coupled to the internal stress level. When the internal stress is decreased, the microcracking length is increased, since the equivalent Von Mises shear stress will be reached for higher applied loads. To summarize, the microcracking phenomenon allows a release of internal stresses; the length of the joint could therefore be reduced by a length approximately equal to that of the microcracked zone without affecting its performance.

While this case is the most commonly encountered and describes the failure of joints built with brittle adhesives, it is worth mentioning that similar stress-strain curves are obtained when the adhesive is allowed to plasticize. More, the local stress analysis required to describe the partial plasticization of the adhesive is the same as that describing microcracking. It is therefore possible to treat these two different phenomena in the same way. Additionally, by keeping constant the rate of propagation of microcracking (plasticization) along the joint, it is

possible to fit the stress-strain curve in **Fig 5** up to point C, and further obtain the microcracking (plasticization) length, comparing well with the experiment.

## CONCLUSIONS

A new double-lap shear geometry testing was introduced, enhancing the traditional lap-shear test resolution. Using a modified shear-lag theory, the axial and shear stresses were determined in the adherents and adhesive, including the effects of internal stresses, using a simple formalism. It was further shown that internal stresses contribute to a great extent to reducing the strength of the joint and therefore must be accounted for. This analysis was further expanded to include effects of adhesive cohesive failure (microcracking) prior to interfacial debonding.

## REFERENCES

1. Anderson, G.P. and K.L. DeVries, 1989. in *Treatise on Adhesion and Adhesives*, R.L. Patrick, Marcel Dekker, Inc: NY & Basel: p. 55.
2. Volkersen, O., 1938. *Luftfahrtforschung*, **15**: p. 41.
3. Goland, M. and E. Reissner, 1944. *J. Appl. Mech.*, **11**: p. A17-A27.
4. Mendels, D.-A., Y. Leterrier, and J.-A.E. Manson, 1999. in *proc. of DURACOSYS'99*, Brussels: july 11-14.
5. Nairn, J.A. and D. A. Mendels, 2000. *Mechanics of Materials.*, submitted
6. Mendels, D.-A., Y. Leterrier, and J.-A.E. Manson, 1999. *J. Compos. Mater.*, **33**: p. 1525.
7. Page, S. A., D.-A. Mendels, L. Boogh, J.-A.E. Manson, 1999. *ECCM'9*, submitted
8. Gilibert, Y., M.L.L. Klein, A. Rigolot, 1986. *Rapport de Recherche 207, ENSTA (France)*.

## ACKNOWLEDGEMENTS

The authors are indebted to the Swiss National Science Foundation for financial support.

Table I: Material and geometric properties of the system studied

Layer	Material	$E_y$ (GPa)	$\nu_{xy}$	$\alpha$ ( $10^{-5} 1/K$ )	$t$ (mm)
1 & 3	Aluminum	69	0.33	2.36	4
2	Epoxy	3.167	0.35	6.70	0.2

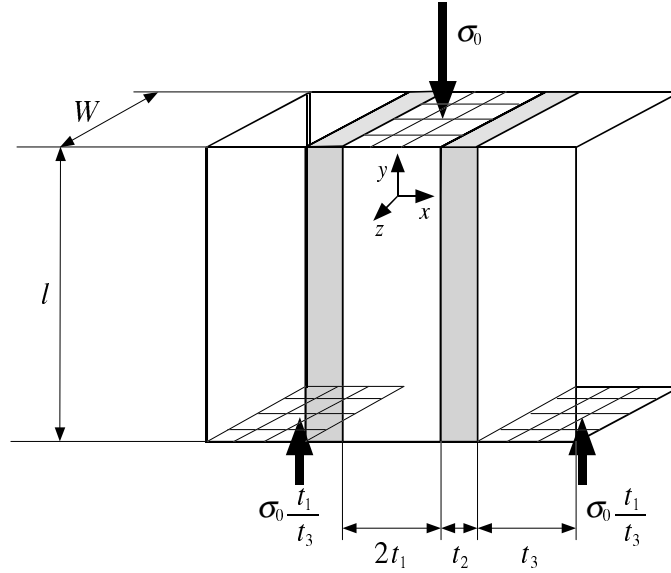


Figure 1: Geometry of the modified double lap-shear specimen

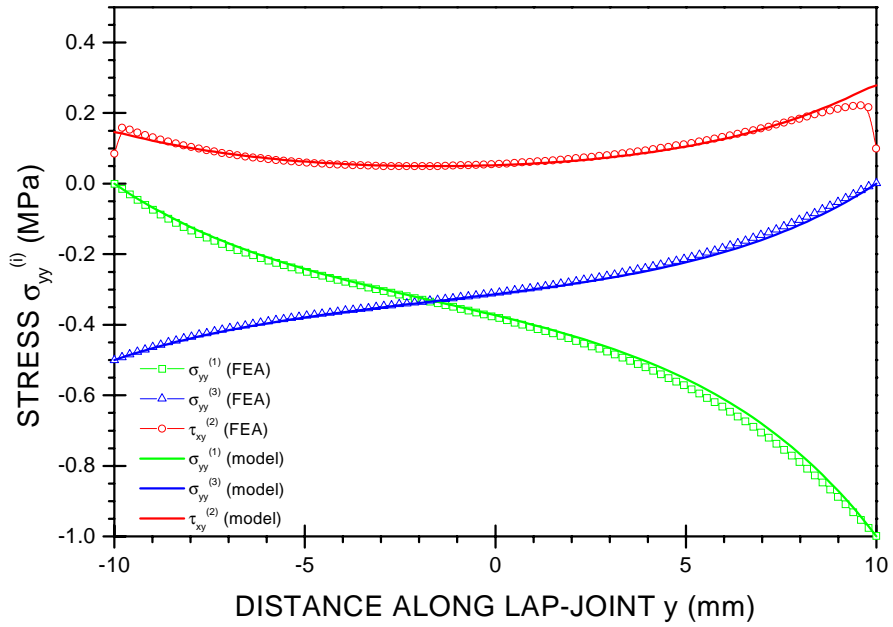


Figure 2: Axial and shear stresses vs. distance along lap-joint, solution with hyperbolic shape functions,  $\Delta T=0^\circ\text{C}$ ,  $\sigma_0 = 1\text{MPa}$

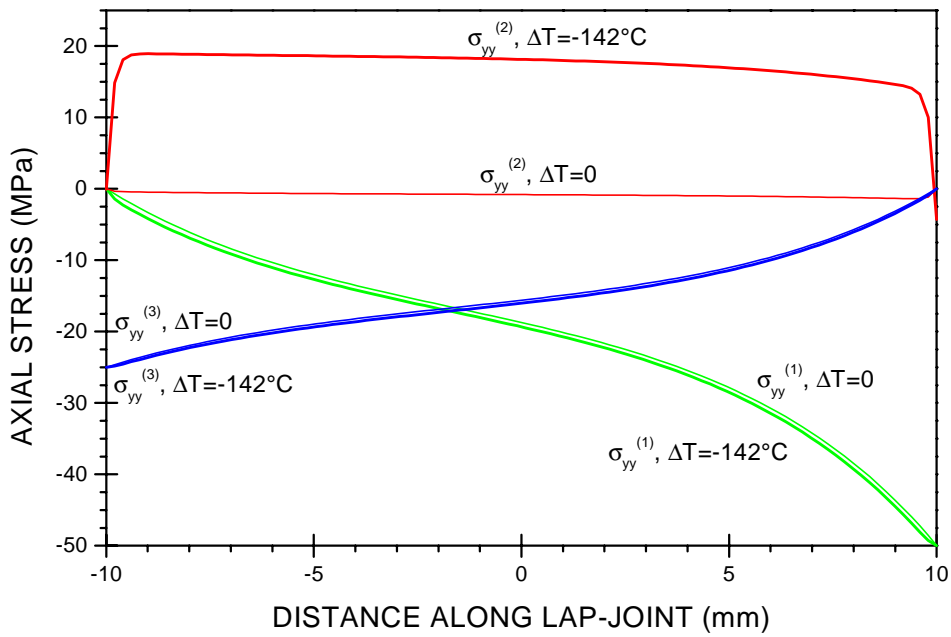


Figure 3: Axial stresses vs. distance along lap-joint, solution with hyperbolic shape functions, including internal stresses,  $\Delta T = -142^\circ\text{C}$ ,  $\sigma_0 = 50\text{MPa}$

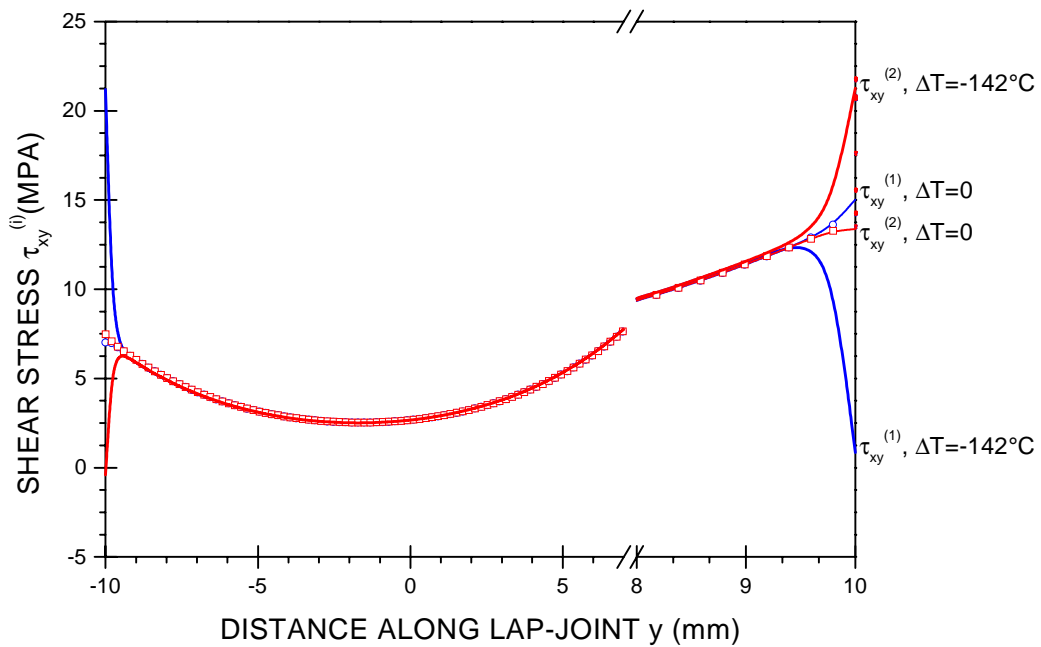


Figure 4: Shear stresses vs. distance along lap-joint, solution with hyperbolic shape functions, including internal stresses,  $\Delta T = -142^\circ\text{C}$ ,  $\sigma_0 = 50\text{MPa}$

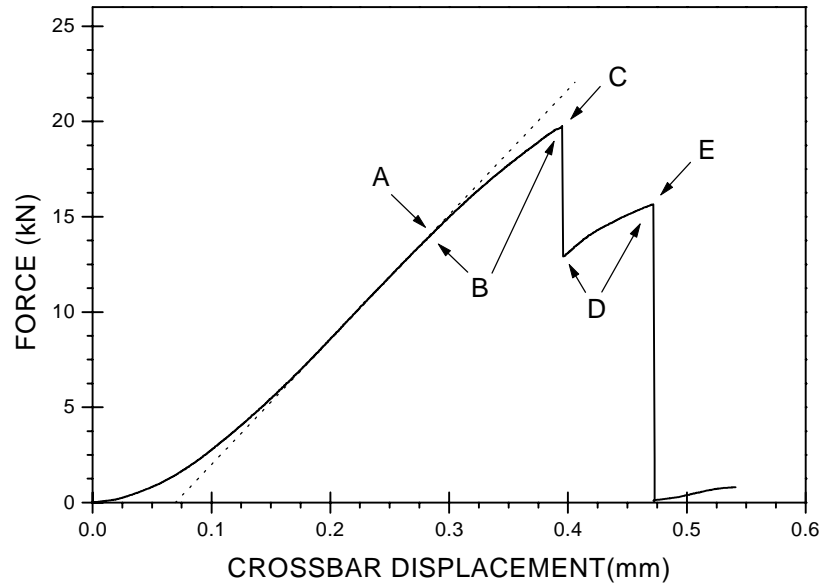


Figure 5: Typical force vs. displacement curve obtained during the testing in compression of a modified double-lap shear specimen: A. microcracking onset; B. Microcracking propagation in both adhesive joints; C. Interfacial failure of the first adhesive joint; D. Microcracking propagation in the second adhesive joint; E. Interfacial fracture of the second adhesive joint

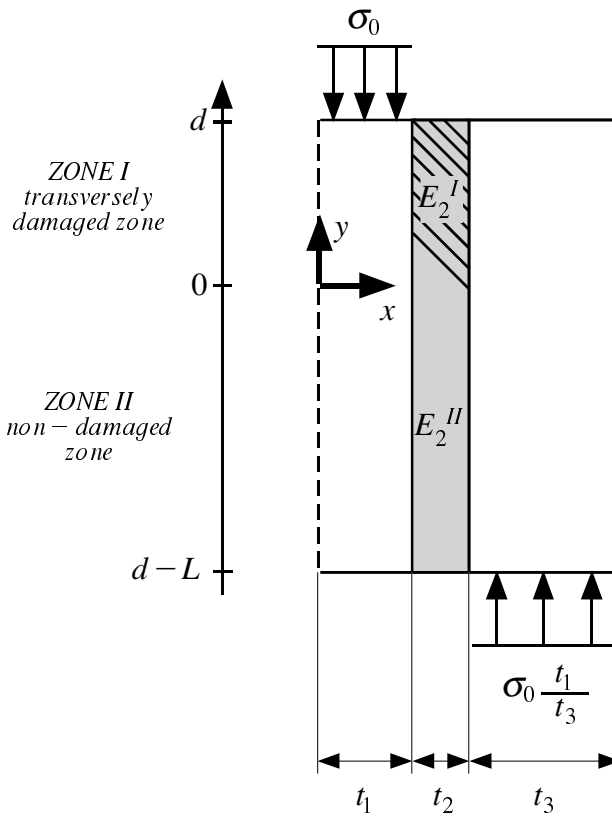


Figure 6: Model system with a zone of transversely cracked adhesive of length  $d$

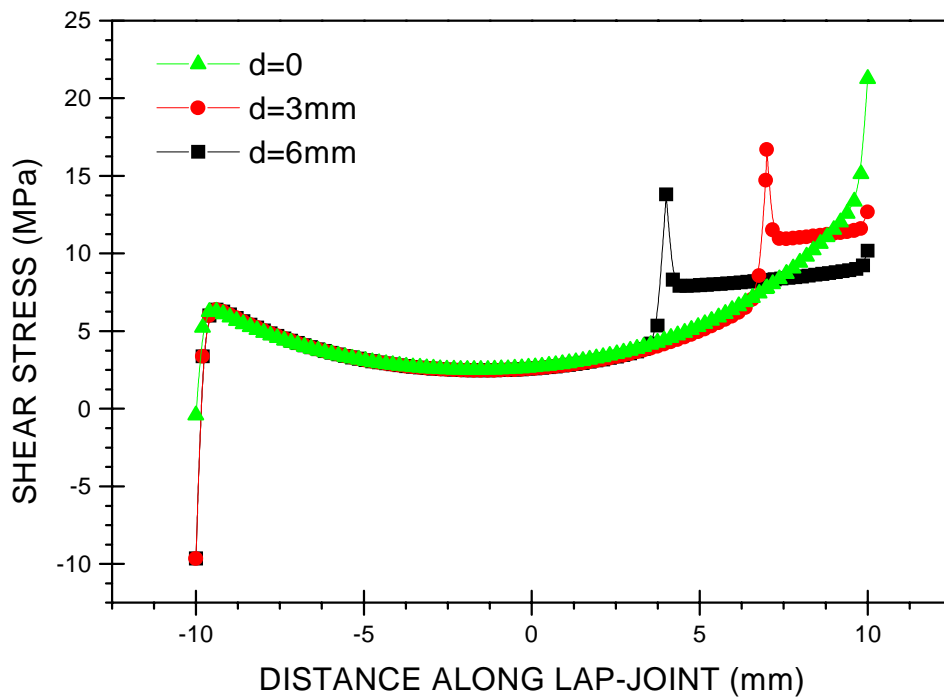


Figure 7: Stresses vs. distance along lap-joint, with a damage zone of length  $d = 0, 3, 6$  mm, Young's modulus  $E_2^I = 0.1 E_2^{II}$ , internal stresses:  $\Delta T = -142^\circ\text{C}$ ,  $\sigma_0 = 50\text{MPa}$